NANO LETTERS

Letter

pubs.acs.org/NanoLett

Sulfur Nanocrystals Confined in Carbon Nanotube Network As a Binder-Free Electrode for High-Performance Lithium Sulfur Batteries

Li Sun, Mengya Li, Ying Jiang, Weibang Kong, Kaili Jiang, Jiaping Wang,* and Shoushan Fan

Department of Physics and Tsinghua-Foxconn Nanotechnology Research Center, Tsinghua University, Beijing, People's Republic of China, 100084

Supporting Information

ABSTRACT: A binder-free nano sulfur−carbon nanotube composite material featured by clusters of sulfur nanocrystals anchored across the superaligned carbon nanotube (SACNT) matrix is fabricated via a facile solution-based method. The conductive SACNT matrix not only avoids self-aggregation and ensures dispersive distribution of the sulfur nanocrystals but also offers three-dimensional continuous electron pathway, provides sufficient porosity in the matrix to benefit electrolyte infiltration, confines the sulfur/polysulfides, and accommodates the volume variations of sulfur during cycling. The nanosized sulfur particles shorten lithium ion diffusion path, and the confinement of sulfur particles in the SACNT network guarantees the stability of structure and electrochemical performance of the composite. The nano S-SACNT composite cathode delivers an initial discharge capacity of 1071 mAh g^{-1}, a peak capacity of 1088 mAh g^{-1}, and capacity retention of 85% after 100 cycles with high Coulombic efficiency (~100%) at 1 C. Moreover, at high current rates the nano S-SACNT composite displays impressive capacities of 1006 mAh g^{-1} at 2 C, 960 mAh g^{-1} at 5 C, and 879 mAh g^{-1} at 10 C.

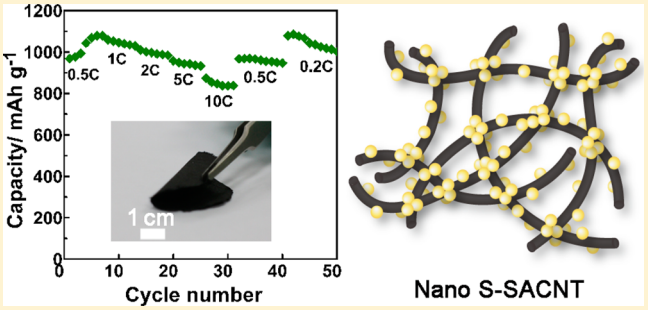

KEYWORDS: *Sulfur−carbon composite, carbon nanotube, binder-free electrode, lithium sulfur battery*

Traditional lithium-ion batteries (LIBs) have reached their bottlenecks in the applications of energy storage in portable electronic devices and electric vehicles (EVs) due to their limited capacity.[1−4] Current LIBs with transition metal oxide as the cathode and graphite as the anode deliver limited capacity of ~200 mAh g^{-1} and energy density of ~150 Wh kg^{-1}, which are still far from the requirement of EVs in future application. Extensive researches beyond LIBs have been widely carried out in order to develop new and emerging rechargeable batteries with higher energy density,[5−8] among which lithium−sulfur (Li−S) battery stands out as a promising candidate.[9,10] Li−S batteries utilize a sulfur cathode and a lithium metal anode. Though with a relatively low average potential of 2.15 V with respect to Li/Li^+, the sulfur cathode possesses an extremely high theoretical capacity of 1672 mAh g^{-1} and specific energy density of 2567 Wh kg^{-1} through the multielectron-transfer reaction of $S_8 + 16Li^+ + 16e^{-1} \rightarrow 8Li_2S$.[11,12] Moreover, sulfur is considered more suitable for commercialization due to its nontoxicity, low cost, being environmentally benign, and abundance in nature. However, despite of these promises, the development of practical Li−S batteries has been hindered by several issues. The inherent insulating nature of sulfur (5×10^{-30} S cm^{-1} at room temperature) inevitably causes low active material utilization and poor rate capability. Severe volumetric expansion/shrinkage (~80%) of sulfur during charge/discharge processes gradually decreases the mechanical integrity and the stability of electrode over long cycles. In addition, the redox chemistry of sulfur in the cathode is relied on a solid (S_8)−liquid (polysulfides, S_{4-8}^{2-})−solid (Li_2S/Li_2S_2) reaction, in which the intermediate polysulfide ions are soluble in the liquid electrolyte, resulting in loss of active materials. Moreover, the dissolved polysulfides travel between the electrodes during cycling, being oxidized and reduced on both electrodes. Such a redox shuttle effect brings critical problems including decrease of Coulombic efficiency and capacity decay due to the insulating Li_2S/Li_2S_2 deposited on both electrodes.

One strategy to solve the above issues is to confine elemental sulfur in a porous and conductive carbon matrix, which cannot only function as a conductive pathway but also provide efficient physical confinement or chemical bonding to trap the soluble polysulfides during cycling. Various carbon hosts were designed in literature, mostly with a micro/meso porous structure, including porous graphitic carbon,[13] porous hollow carbon,[14] disordered carbon nanotubes (CNTs),[15] double-shelled hollow carbon spheres,[16] spherical ordered mesoporous carbon nanoparticles,[17] microporous−mesoporous carbon with graphitic structure,[18] and so forth. Nevertheless, in order to incorporate sulfur into the micro/meso pores of the carbon matrix, thermal treatment (155 °C or higher) for a long time

Received: April 22, 2014
Revised: May 22, 2014
Published: June 2, 2014

(12 h or more) is needed to allow the solid sulfur to melt and diffuse into these pores. The complex procedures to prepare these special carbon structures and the following thermal treatment require a large consumption of energy. Additionally, tortuous pores within the electrodes may impede the electrolyte infiltration and limit the kinetics of the charge−discharge reactions due to the relatively small diffusion coefficient combined with long diffusion paths, which reduce sulfur utilization and hinder high-rate performance. Moreover, considering sulfur can diffuse into the designed pores in the carbon matrix, polysulfides can also transfer through the same path over long cycles, and the confinement by the porous structure may be vanished.

In order to increase the utilization efficiency of the active material, promote the electrolyte infiltration throughout the electrode, and benefit the high-rate performance of Li−S batteries, a more open carbon−sulfur composite structure that can still exert its function in confining sulfur and polysulfides should be a good choice for carbon−sulfur cathodes. Carbon nanotubes (CNTs) have been extensively studied as conductive matrix to load sulfur due to their large specific surface area and abundant active sites.[19−21] Though more open porous structures formed by CNTs greatly improved electrolyte infiltration, limited capacities were obtained in these CNT−sulfur composites, mainly due to the relatively weak confinement of sulfur and polysulfides by CNTs. Herein, based on superaligned CNTs (SACNTs),[22] we report the rational design and facile synthesis of a new nano S-SACNT composite without additional binders or conductive additives by confining sulfur in the flexible SACNT matrix. In comparison with ordinary CNTs, SACNTs exhibit "super-aligned" nature, large aspect ratio (~10^4), clean surface, and strong van der Waals force among tubes and bundles. When being dispersed in solvent by ultrasonication, SACNT bundles were expanded into a continuous and three-dimensional conductive network with highly open and porous structure. The nano S-SACNT composite is featured with uniform clusters of sulfur nanocrystals surrounding SACNTs. Different from those complex porous structures that intend to confine sulfur via torturous micropores or dense coatings, the highly porous and conductive three-dimensional (3D) SACNT matrix was more efficient for the transfer of electron, infiltration of electrolyte, and accommodation of volume variation. The 3D SACNT network can also alleviate the loss of polysulfides by offering numerous adhesion points and continuous physical barriers to trap the final lithiation product (Li_2S/Li_2S_2) of polysulfides, and therefore confine the cathode reaction within the electrode and avoid overaggregation of sulfur/Li_2S/Li_2S_2. Besides, the uniform distribution of sulfur nanocrystals in the SACNT matrix is achieved under room temperature and ambient pressure without performing any complex procedures or utilizing any toxic materials, which is simple, fast, and energy-preserving.

The solution-based fabrication process and detailed structure of the nano S-SACNT composite are schematically illustrated in Figure 1a. Elemental sulfur, which is nonpolar, was dissolved in one nonpolar solvent (ethanol used here) with intensive ultrasonication. SACNT arrays were dispersed in the sulfur-ethanol solution by ultrasonication and expanded into a continuous and 3D network with volume at least 100 times larger than that of the original SACNT arrays (Figure 1b), indicating the large porosity inside. With the addition of the other polar solvent (DI water used here), sulfur particles

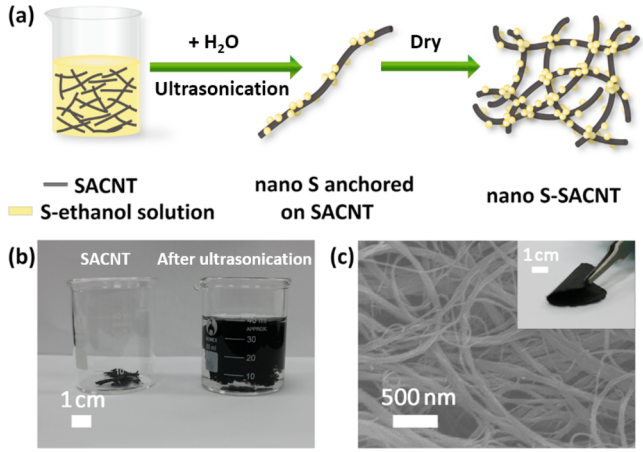

Figure 1. (a) Schematic of the synthesis procedure of the nano S-SACNT composite. (b) A photograph showing the volume expansion of SACNTs (10 mg) in solution after ultrasonication. (c) SEM image of the nano S-SACNT composite. The inset of (c) gives a photograph of the binder-free nano S-SACNT composite.

precipitated from the solution and deposited on the well-dispersed SACNT network that provides abundant adhesion points for sulfur deposition. Note that the DI water should be added dropwise at a slow speed in order to allow all the generated sulfur to uniformly anchor on SACNTs without self-aggregation. Under an optimized condition, sulfur nanoparticles can deposit conformally along the outer surface of SACNTs forming a nano S-SACNT composite as a flexible and binder-free electrode after drying (the inset of Figure 1c). The SACNT network in the solution plays an important role in preventing the growth and aggregation of sulfur, resulting in nanosized sulfur particles anchored on SACNTs. The scanning electron microscopy (SEM) image (Figure 1c) of the nano S-SACNT composite turns out to be almost the same morphology as that of pure SACNT network without any sulfur aggregations. As a contrast, without SACNT in the solution, large sulfur particles (micro S, 10−30 μm) were formed due to an open environment and consequently severe self-aggregation, as shown in Supporting Information Figure S1d. The micro S was mixed with conductive additive and binder and then casted onto an alumina foil to form a traditional micro S-CB electrode as a control sample.

The detailed structure and composition of the nano S-SACNT composite were investigated by X-ray diffraction (XRD) and thermogravimetric analysis (TGA). Figure 2a shows the XRD patterns of the nano S-SACNT composite and the pure SACNT. The characteristic diffraction peak (002) of CNT was observed at 26° in both samples. All the other diffraction peaks of the nano S-SACNT composite correspond to those of the *Fddd* orthorhombic sulfur (S_8, PDF#08-0247) plotted by the column red lines, indicating that sulfur in the SACNT network is crystalline without formation of any carbon−sulfur compounds during the fabrication process. An average sulfur crystallite size of 34.7 nm was revealed in the nano S-SACNT sample based on the (040) plane in the XRD profile according to the Scherrer's equation.[23]

TGA curves of the nano S-SACNT composite and pure sulfur are shown in Figure 2b. Both samples exhibited continuous weight loss at temperatures between 150 and 260 °C, corresponding to the oxidation of sulfur in air. The nano S-SACNT composite showed a weight loss of approximately 50%,

dx.doi.org/10.1021/nl501486n | *Nano Lett.* 2014, 14, 4044−4049

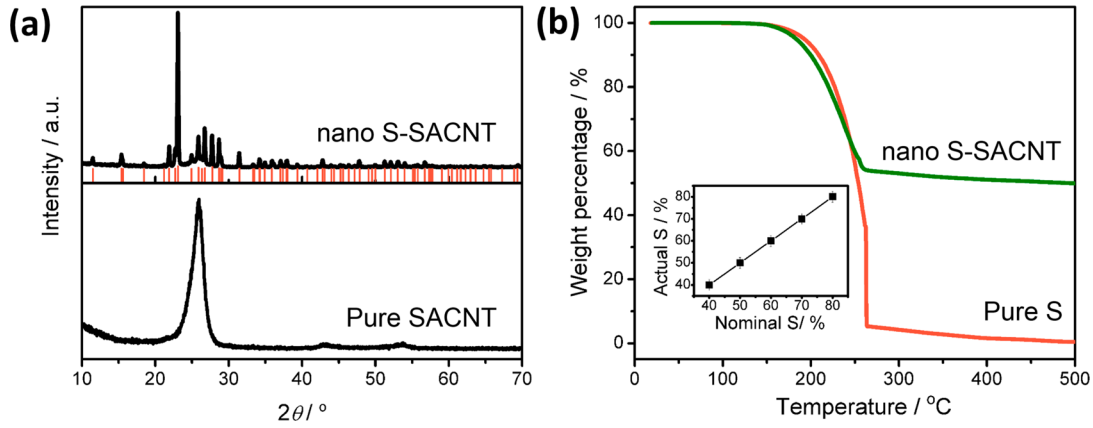

Figure 2. (a) XRD spectra of nano S-SACNT and pure SACNT. (b) TGA curves of nano S-SACNT and pure S. The inset of (b) shows the linear correlation between nominal sulfur and actual sulfur content in the composites.

and therefore the sulfur loading in this composite was identified as 50%. We prepared S-SACNT composites with various sulfur loading, and the actual sulfur contents measured by TGA in the obtained composites agree well with those normalized in the raw materials. Even when the sulfur addition reached as high as 80%, almost no weight loss was found during the fabrication process, contributing to the high sulfur yield in the nano S-SACNT composite (the inset of Figure 2b). The controllability of sulfur content in composite is of great advantage over those complex synthesis methods reported in literature.

Figure 3a shows the transmission electron microscopy (TEM) image of the as-prepared nano S-SACNT composite. Clusters of sulfur nanocrystals anchor uniformly across the SACNT network. The TEM image of an individual SACNT loaded with sulfur nanocrystals in Figure 3b shows that the diameter of the SACNTs is about 10 nm, and the sulfur nanocrystals surrounding the SACNTs are mostly with a grain size of 10−20 nm, roughly in accordance with that estimated from the XRD pattern. The energy-dispersive X-ray spectroscopy (EDS) line spectra of element C and S perpendicular to the SACNT walls in Figure 3b proves the existence of sulfur surrounding the outer surface of the SACNT, and the consistent sulfur signal in the region marked by the red frame (shown in the inset) indicates the uniform distribution of sulfur. In the nano S-SACNT composite, instead of being confined in pores or by shells, sulfur anchored on the surface of the conductive SACNTs can effectively access the electrolyte for efficient lithium ion transfer and increase the utilization of the active material.

The structure of the anchored sulfur nanoclusters can be well resolved in the high-magnification TEM image (Figure 3c). The green dash lines mark the edges of the SACNTs, and the distance between the multiwalls of the SACNTs is 0.34 nm, corresponding to their characteristic (002) peak in the XRD pattern. The selected region marked by the red dash lines in Figure 3c is zoomed in to examine the detailed structure of the composite (Figure 3d). Mutual 0.344/0.321 nm lattice fringes with an intersection angle of around 120° corresponding to the (026)/(040) planes are observed in the sulfur nanocrystals, which reflect the well-defined crystalline structure of sulfur. The lattice fringes of sulfur nanocrystals extend into the region of the SACNT marked by the green dash lines, which confirms that SACNTs are surrounded by a layer of sulfur nanocrystals.

Figure 3e and Supporting Information Figure S1e show the scanning electron microscope (SEM) images of the top surface

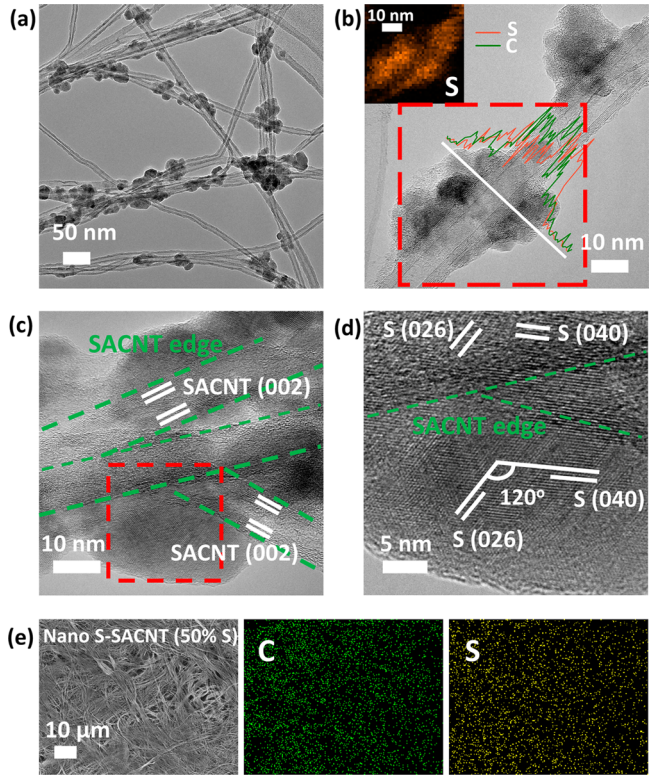

Figure 3. (a,b) TEM images of the nano S-SACNT composite, showing sulfur nanocrystals loaded on SACNTs. The EDS line scanning perpendicular to the SACNT walls and area mapping of the selected region are given in (b) and its inset. (c,d) High-resolution TEM images showing clear lattice fringes of sulfur and the S/SACNT interface. (e) SEM image of the nano S-SACNT composite and the corresponding EDS mapping of carbon and sulfur.

and the cross section of the nano S-SACNT composite electrode. Large sulfur particles are not observed in the image, indicating no agglomeration of sulfur nanocrystals. The EDS data indicates that sulfur and carbon were the only elements present in the nano S-SACNT composite. EDS mapping demonstrates uniform distributions of elemental carbon and sulfur in this area, suggesting that the sulfur nanoparticles were embedded homogeneously in the conductive SACNT network. Carbon (Supporting Information Figure S1b) and sulfur (Supporting Information Figure S1c) elemental mapping of

dx.doi.org/10.1021/nl501486n | *Nano Lett.* 2014, 14, 4044−4049

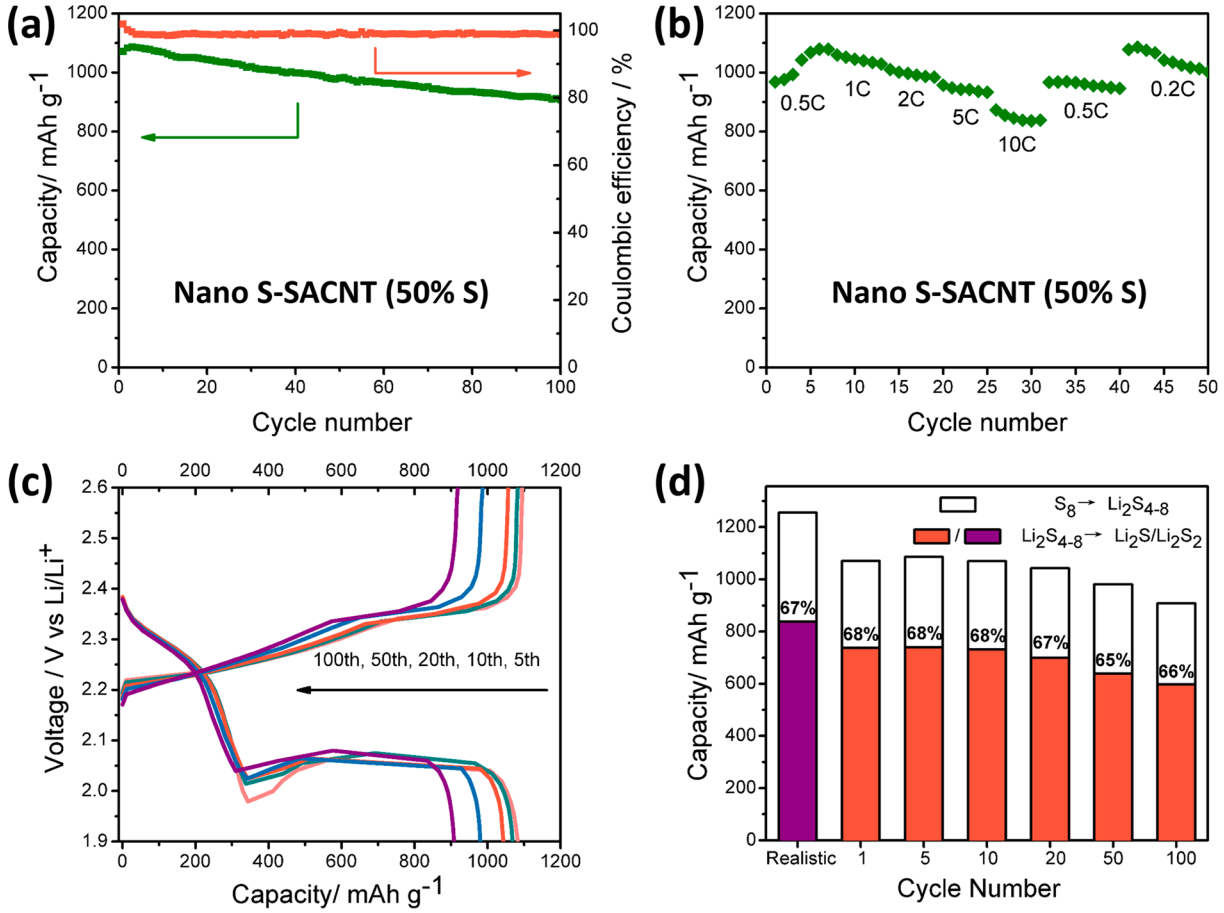

Figure 4. Electrochemical characterization of the nano S-SACNT composite. (a) Cycling performance at charge/discharge rate of 1 C/1 C. (b) Rate performance. (c) Charge and discharge voltage profiles at 5th, 10th, 20th, 50th, and 100th cycle. (d) Capacity contribution of the reaction from polysulfides to Li_2S/Li_2S_2 in the discharge capacities at 1 C.

the edge of the sample (Supporting Information Figure S1a) was also given, and no sulfur was found in the region of the sample holder, eliminating the influence of sulfur signal from the background. Therefore, we can conclude that during solvent evaporation, the deposited sulfur nanocrystals remained anchoring on the SACNT surface and did not aggregate into large clusters. Besides, the bushy SACNT network formed by removal of solvent provides numerous adhesion points to trap the intermediate polysulfides and their lithiation product. This will confine the cathode reaction within the nano S-SACNT electrode, alleviate the loss of active materials, minimize the shuttle effect, and therefore enhance the structure and performance reversibility of the electrode.

Note that the particle size of sulfur is highly related to its percentage in the composite. Composites with higher sulfur loading were prepared by the same procedure. When the sulfur loading increased to 60%, sulfur aggregates of around 1 μm were found in the SEM image, as marked by the white arrows in Supporting Information Figure S1f. Further increase of sulfur content up to 80% resulted in more and larger sulfur aggregates, as shown in Supporting Information Figure S1g. These larger sulfur aggregates will decrease the utilization of active material in the composite.

The nano S-SACNT composites exhibited high reversible capacities and stable cycling performance. At the charge/discharge rates of 1 C/1 C (1 C = 1672 mA g^{-1}), a high initial specific capacity of 1071 mAh g^{-1} was obtained, with Coulombic efficiency stabilized around 100% in the subsequent cycles (Figure 4a). A slight increase of the capacity was found in the first four cycles, which was possibly attributed to the initial wetting process between electrode and electrolyte and a consequent maximization of the cathode utilization. The electrochemical impedance spectra presented in Supporting Information Figure S2a further confirm such initial activation process of the electrode. After sufficient activation, the cell reached its peak capacity of 1088 mAh g^{-1}. Even after 100 cycles, a capacity as high as 909 mAh g^{-1}, corresponding to a high capacity retention of 85%, was exhibited. The stable cycling performance of nano S-SACNT composite is of great advantage over the traditional micro S-CB electrode (Supporting Information Figure S3), which exhibited small initial capacities of 621 mAh g^{-1}, low Coulombic efficiencies (<80%), and capacity retention of only 65% after 100 cycles. The superiority of the nano S-SACNT cathode is ascribed to the uniform distribution of nanosized sulfur particles on SACNTs to allow sufficient utilization of active materials, the relatively open structure of SACNT network to facilitate easy electrolyte infiltration, and the numerous adhesion points provided by the SACNT network to trap the polysulfides and their lithiation product. The nano S-SACNT composites displayed impressive cycling performance comparing to recently reported binder-free sulfur−carbon electrodes with similar sulfur content, such as the fibrous hybrid of graphene and sulfur nanocrystals that exhibited capacities of around 700 to 541 mAh g^{-1} at 0.5 C in

dx.doi.org/10.1021/nl501486n | *Nano Lett.* 2014, 14, 4044−4049

100 cycles[24] and the flexible nanostructured sulfur-CNT cathode that showed capacities of 653 to 524 mAh g^{-1} at 1 C in 100 cycles.[25]

Benefiting from the high conductivity of the SACNT network and the nanoscale dimension of sulfur particles, the nano S-SACNT composite also showed favorable high-rate capability. As shown in Figure 4b, at a constant discharge current of 0.5 C, the composite demonstrated a stepwise capacity of 970−1088, 1062−1026, 1006−992, 960−934, and 879−842 mAh g^{-1} at charge current of 0.5, 1, 2, 5, and 10 C, respectively, significantly higher than those reported for Li−S batteries in literature.[13−21] Similarly, a slight increase was found in the first few cycles at 0.5 C, corresponding to the activation process of the electrode. Moreover, after the high-rate charge/discharge process, when the same cell was then cycled at charge/discharge rates of 0.5 C/0.5 C and following rates of 0.2 C/0.2 C, large capacities of 965−945 mAh g^{-1} and 1077−1016 mAh g^{-1} could still be delivered, implying good reversibility of the composite.

The galvanostatic charge−discharge behavior of the nano S-SACNT cathode at charge/discharge rates of 1 C/1 C was also evaluated within the voltage window of 1.9−2.6 V versus Li^+/Li (Figure 4c). Consistent with the two cathodic peaks at 2.3 and 2.03 V in the cyclic voltammetry (Supporting Information Figure S2b), two-plateau behavior of the sulfur cathode was observed, corresponding to the redox reaction from elemental S_8 to polysulfides (S_{4-8}^{2-}) at around 2.3 V and the deep redox reaction to solid Li_2S_2/Li_2S at 2.0 V, respectively. Because the polysulfides ions are soluble, the reaction in the first plateau is fast and corresponds to a theoretical capacity of 418 mAh g^{-1}. Continuing discharge will reduce the polysulfides ions to insoluble Li_2S/Li_2S_2, leading to much slower reaction kinetics at the second plateau and the tail. It has been considered that the theoretical value usually cannot be achieved by the second plateau and a lower capacity of 1256 mA h g^{-1} for the sulfur cathode is more realistic (corresponding to 1.5 e S^{-1}).[9] The realistic separate capacity contributions of the two-plateau reactions, i.e., S_8 to polysulfides (Li_2S_{4-8}) and polysulfides (Li_2S_{4-8}) to Li_2S/Li_2S_2, are plotted in the first column in Figure 4d in which the latter (in purple) contributed 67% of the overall capacity. During the discharge process, inevitable dissolution of polysulfides into the electrolyte will cause severe capacity loss for the reaction from polysulfides to Li_2S/Li_2S_2, characterized by the gradual shortening of the second plateau at 2.0 V in the discharge curves. In order to evaluate the loss of polysulfides in the electrode during cycling, we examined the capacity contributions of the reactions from Li_2S_{4-8} to Li_2S/Li_2S_2 in the nano S-SACNT composite for increased cycling numbers (Figure 4d). The initial discharge capacity at the current rate of 1 C was 1071 mAh g^{-1} of which 68% (737 mAh g^{-1}) was assigned to the transition from polysulfides to Li_2S/Li_2S_2. The contribution of the polysulfides-Li_2S/Li_2S_2 reaction remained stable during the cycling. The corresponding percentages for the 5th, 10th, 20th, and 50th cycles were 68, 68, 67, and 65%, respectively. Even in the 100th cycle, the second plateau could still attribute to 66% (598 mAh g^{-1}) of the overall capacity. The large and stable capacity contribution by the second plateau reflects sufficient reaction of the intermediate polysulfides and effective utilization of sulfur in the SACNT matrix. This further confirms that the SACNT network not only offers efficient electrolyte infiltration to exert large sulfur utilization but also confines sulfur/polysulfides and alleviates loss of active material that ensures the excellent electrochemical stability of the nano S-SACNT composite electrode.

The morphology of the nano S-SACNT composite electrode after 100 cycles at 1 C was studied by SEM. In Supporting Information Figure S1h, no mechanical crack or large agglomerate of insulating Li_2S/Li_2S_2 was found on the surface of the composite electrode. The EDS mapping of the electrodes in Supporting Information Figure S1i shows that sulfur existed throughout the electrode, which directly proves that the SACNT framework architecture prevents agglomeration of electrode material and provides effective confinement to sulfur/polysulfides to enhance the electrochemical performance of the electrode.

The excellent electrochemical performances of the nano S-SACNT composite are ascribed to the special framework of the SACNTs and the uniform distribution of nanoscale sulfur clusters within it. The 3D SACNT network functions in various aspects: (1) its bushy network avoids agglomeration of the synthesized sulfur nanocrystals and their lithiation product Li_2S/Li_2S_2, which is beneficial to maintain a uniform and stable electrode structure; (2) its high conductivity greatly enhances the electric conductivity of the composite and benefits the charge transfer; (3) its flexibility ensures SACNT network to act as a buffer around the sulfur particles, which remarkably accommodates the volume variations during cycling and avoids destruction of the electrode; (4) its inner porous structure offers easy access of the electrolyte to sulfur nanoparticles, which might be helpful for efficient Li^+ insertion/extraction; and (5) its physical confinement to sulfur/polysulfides alleviates the loss and aggregation of active materials. The unique features of the SACNT network, together with the uniform distribution of sulfur nanocrystals through the network structure, allow efficient utilization of sulfur and contribute to the remarkable properties of the nano S-SACNT composite.

In summary, we developed binder-free nano S-SACNT composites by forming clusters of sulfur nanocrystals anchored around the SACNTs via a facile and energy-preserving solution-based method. Such a special structure could provide a conductive network, accommodate the volume expansion during the cycling, and offer physical confinement of polysulfide intermediates. Moreover, different from those trying to restrict sulfur in rigid and torturous inner pores, the nano S-SACNT composite provides a more open environment to allow sufficient electrolyte infiltration and fast ion transportation, resulting in excellent high-rate performance. The nano S-SACNT composite delivers high specific capacity with 100% Coulombic efficiency and stable cycling performance as the cathode for Li−S batteries. Besides, with appealing performance at higher charge/discharge rates the nano S-SACNT composite is of significant promise for high energy/power density rechargeable batteries.

■ ASSOCIATED CONTENT

Ⓢ Supporting Information

Sample preparation, sample analysis, figures showing SEM and EDS images, EIS spectra, cyclic voltammogram, and electrochemical performance, and additional references. This material is available free of charge via the Internet at http://pubs.acs.org.

■ AUTHOR INFORMATION

Corresponding Author

*E-mail: jpwang@tsinghua.edu.cn.

Notes

The authors declare no competing financial interest.

■ ACKNOWLEDGMENTS

This work was supported by the National Basic Research Program of China (2012CB932301) and the NSFC (51102146). The authors declare no competing financial interest.

■ REFERENCES

(1) Cairns, E. J.; Albertus, P. *Annu. Rev. Chem. Biomol. Eng.* **2010**, *1*, 299−320.
(2) Goodenough, J. B.; Kim, Y. J. *Power Sources* **2011**, *196*, 6688−6694.
(3) Whittingham, M. S. *MRS Bull.* **2008**, *33*, 411−419.
(4) Ellis, B. L.; Lee, K. T.; Nazar, L. F. *Chem. Mater.* **2010**, *22*, 691−714.
(5) Cai, K.; Song, M. K.; Cairns, E. J.; Zhang, Y. *Nano Lett.* **2012**, *12*, 6474−6479.
(6) Takeuchi, T.; Sakaebe, H.; Kageyama, H.; Senoh, H.; Sakai, T.; Tatsumi, K. J. *Power Sources* **2010**, *195*, 2928−2934.
(7) Yang, Y.; McDowell, M. T.; Jackson, A.; Cha, J. J.; Hong, S. S.; Cui, Y. *Nano Lett.* **2010**, *10*, 1486−1491.
(8) Hassoun, J.; Scrosati, B. *Angew. Chem., Int. Ed.* **2010**, *49*, 2371−2374.
(9) Wang, D. W.; Zeng, Q.; Zhou, G.; Yin, L.; Li, F.; Cheng, H. M.; Gentle, I. R.; Lu, G. Q. M. *J. Mater. Chem. A* **2013**, *1*, 9382−9394.
(10) Song, M. K.; Cairns, E. J.; Zhang, Y. *Nanoscale* **2013**, *5*, 2186−2204.
(11) Bruce, P. G.; Freunberger, S. A.; Hardwick, L. J.; Tarascon, J. M. *Nat. Mater.* **2012**, *11*, 19−29.
(12) Ji, X. L.; Nazar, L. F. J. *Mater. Chem.* **2010**, *20*, 9821−9826.
(13) Wang, D. W.; Li, F.; Liu, M.; Lu, G. Q.; Cheng, H. M. *Angew. Chem., Int. Ed.* **2008**, *47*, 373−376.
(14) Jayaprakash, N.; Shen, J.; Moganty, S. S.; Corona, A.; Archer, L. A. *Angew. Chem., Int. Ed.* **2011**, *50*, 5904−5908.
(15) Guo, J.; Xu, Y.; Wang, C. *Nano Lett.* **2011**, *11*, 4288−4294.
(16) Zhang, H.; Wu, H. B.; Yuan, C.; Guo, Z.; Lou, X. W. *Angew. Chem., Int. Ed.* **2012**, *51*, 9592−9595.
(17) Schuster, J.; He, G.; Mandlmeier, B.; Yim, T.; Lee, K. T.; Bein, T.; Nazar, L. F. *Angew. Chem., Int. Ed.* **2012**, *51*, 3591−3595.
(18) Wang, D. W.; Zhou, G.; Li, F.; Wu, K. H.; Lu, G. Q.; Cheng, H. M.; Gentle, I. R. *Phys. Chem. Chem. Phys.* **2012**, *14*, 8703−8710.
(19) Zheng, W.; Liu, Y. W.; Hu, X. G.; Zhang, C. F. *Electrochim. Acta* **2006**, *51*, 1330−1335.
(20) Han, S. C.; Song, M. S.; Lee, H.; Kim, H. S.; Ahn, H. J.; Lee, J. Y. J. *Electrochem. Soc.* **2003**, *150*, A889−A893.
(21) Jin, K. K.; Zhou, X. F.; Zhang, L. Z.; Xin, X.; Wan, G. H.; Liu, Z. P. J. *Phys. Chem. C* **2013**, *117*, 21112−21119.
(22) Jiang, K. L.; Wang, J. P.; Li, Q. Q.; Liu, L.; Liu, C. H.; Fan, S. S. *Adv. Mater.* **2011**, *23*, 1154−1161.
(23) Patterson, A. *Phys. Rev.* **1939**, *56*, 978−982.
(24) Zhou, G.; Yin, L.; Wang, D. W.; Li, L.; Pei, S.; Gentle, I. R.; Li, F.; Cheng, H. M. *ACS Nano* **2013**, *7*, 5367−5375.
(25) Zhou, G.; Wang, D. W.; Li, F.; Hou, P. X.; Yin, L.; Liu, C.; Lu, G. Q.; Gentle, I. R.; Cheng, H. M. *Energy Environ. Sci.* **2012**, *5*, 8901−8906.